JOURNAL OF GEOPHYSICAL RESEARCH, VOL. 102, NO. A6, PAGES 11,429–11,441, JUNE 1, 1997

Association of waves with narrow particle dropouts in the outer radiation belt

W. L. Imhof,[1] J. Mobilia,[1] H. D. Voss,[1,2] H. L. Collin,[1] M. Walt,[3]
R. R. Anderson,[4] and J. R. Wygant[5,6]

Abstract. An investigation has been made of the association of plasma waves with narrow dropouts (<30-min observation time) in the fluxes of trapped energetic electrons and protons within the radiation belts. The experiment, conducted with instruments on the CRRES satellite, indicates that 5 Hz < frequency < 1 kHz waves are nearly always produced at the times and positions of narrow energetic electron flux dropouts. The waves may be produced at the positions of steep particle flux gradients. This phenomenon is best studied during short-duration events that provide measurements on both sides of a boundary in a relatively quiescent state. In addition to an investigation of the waves associated with narrow dropouts the data presented here show the general correlations between waves and particle fluxes, particularly after new injections or plasmapause crossings. In some cases, energetic proton dropouts also occur and may contribute to the generation of waves.

Introduction

At synchronous or near-synchronous orbit, long-duration (≥30 min) decreases in the fluxes of energetic electrons and protons have been observed followed by very rapid increases [e.g., *Walker et al.*, 1976; *Erickson et al.*, 1979; *Sauvaud and Winckler*, 1980; *Nagai*, 1982; *Baker and McPherron*, 1990; *Baker et al.*, 1993; *Nakamura et al.*, 1994; *Thomsen et al.*, 1994; *Moldwin et al.*, 1995; *Fennell et al.*, 1996]. Most of these decreases have been interpreted as resulting from the relative motion of the satellite with respect to various boundaries such as (1) the outer trapping boundary, (2) the boundary between closed field lines and the open field lines in the tail lobes, or (3) the magnetopause. Flux dropouts associated with the growth phase of substorms have also been attributed to betatron deceleration in the changing geomagnetic field [*Sauvaud et al.*, 1996]. The subsequent flux recoveries, especially cases when the flux increased above the predropout level, have often been associated with the expansion phase onset of magnetospheric substorms. Most of these observations have been made from satellites in geosynchronous orbit, which is nominally at $L = 6.6$.

In addition, short-duration (<30 min) flux dropouts have been observed both at synchronous altitude [*Su et al.*, 1976; *Sergeev et al.*, 1992; *Kopanyi and Korth*, 1995] and on lower L shells [*Yeager and Frank*, 1969; *Kaufmann et al.*, 1972; *Korth et al.*, 1995]. None of the above studies included data on the local plasma wave environment which might be expected to change as the satellites crossed boundaries or encountered currents or strong flux gradients.

The short-duration dropouts at lower L values have not been studied as thoroughly as the more prolonged events, and their source mechanism(s) is (are) not as well understood as those of longer duration. Short-duration events, particularly those in which the particle fluxes return to their predropout values, are more likely due to the transit and subsequent return of the satellite across a plasma boundary than due to a major deformation of the magnetosphere accompanying a substorm injection of particles. In many of the long-duration dropouts the plasma and wave environment at the end of the dropout may be quite different from conditions at the start. Thus the short-duration events offer a better possibility of studying the particle and wave environment on each side of a boundary in a relatively quiescent state.

Waves are known to cause particle precipitation from the radiation belts through wave-particle interactions, but based on the fact that both electrons and protons over a wide range of energies are involved in the dropouts, it is not likely that the particle dropouts are caused by such processes. However, VLF and ELF waves may still play an important role in the overall structure of dropouts. In particular, plasma instabilities such as drift wave instabilities in inhomogeneous plasmas are expected to occur at strong particle flux gradients. Also, electron and ion pitch angle distributions should be different on each side of the plasma boundary, and the waves produced by pitch angle anisotropies should reflect this difference. It is therefore of interest to investigate whether dropouts are associated with the generation of waves in the magnetosphere. The waves can be used as a diagnostic of the boundary motion and of the plasmas involved.

The primary purpose of this paper is to present coordinated data on trapped particle fluxes and plasma wave intensities at the times of narrow particle dropouts. As the comparisons will show, these quantities are not related in any simple way, although simultaneous changes in both particle and wave intensities occur frequently. This research therefore provides data

[1]Lockheed Martin Palo Alto Research Laboratory, Palo Alto, California.
[2]Now at Physics Department, Taylor University, Upland, Indiana.
[3]STARLAB, Stanford University, Stanford, California.
[4]Department of Physics and Astronomy, University of Iowa, Iowa City.
[5]School of Physics and Astronomy, University of Minnesota, Minneapolis.
[6]Formerly at Space Sciences Laboratory, University of California, Berkeley.

Paper number 97JA00462.
0148-0227/97/97JA-00462$09.00

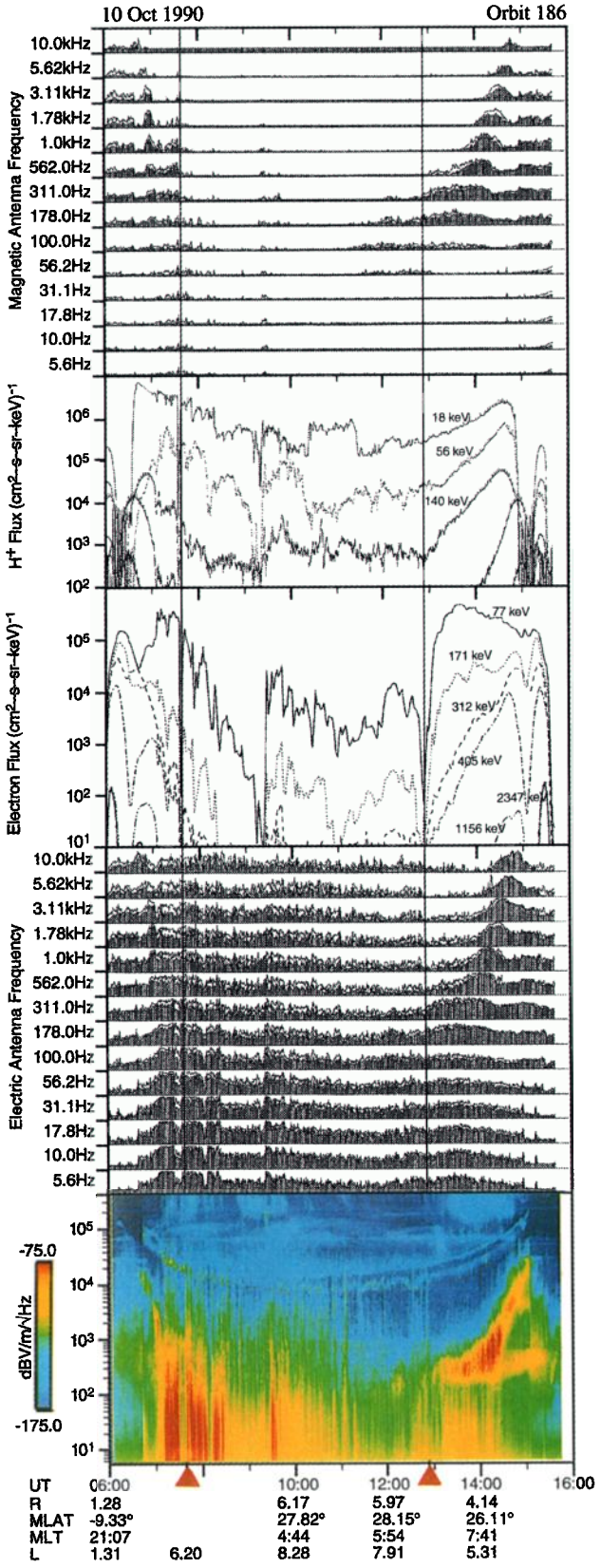

Plate 1. Charged particle and wave data for orbit 186. The bottom sections contain a sweep frequency receiver spectrogram and the output of the multichannel spectrum analyzer for the electric field wave data. Two other sections contain plots of the fluxes of protons and electrons at various energies averaged over the full range of pitch angles. In a top section the magnetic component of the wave data is plotted.

against which theories of wave and particle energy exchange can be tested. Here we make use of VLF and ELF wave and energetic particle measurements performed from the CRRES (Combined Release and Radiation Effects Satellite) which had a highly eccentric, nearly equatorial orbit. The wave environment in and near the regions of narrow particle dropouts is investigated for evidence that the large gradients in particle flux are also regions of enhanced plasma waves. To identify times of observation of particle gradients the entire data set from the spectrometer for electrons and protons (SEP) was surveyed for narrow (<30-min observation time) pronounced dropouts in the electron fluxes within the outer radiation belt. At the times of such events, data from other detectors in the CRRES payload were examined.

Instrumentation

The CRRES satellite was launched on July 25, 1990, into an orbit with an apogee of 35,786 km, a perigee of 350 km, and an inclination of 18°. Apogee at launch was at about 0800 LT, and the spacecraft precessed toward earlier local times at a rate of about 15 hours per year. The satellite spin axis was kept pointed within 15° of the Sun.

The particle data used here were acquired with the ONR 307 instruments on CRRES. One of the instruments in the payload was the spectrometer for electrons and protons. This instrument measured the energy spectra of electrons over the range 40 keV to 5 MeV with silicon solid-state detectors oriented at 80°, 60°, and 40° to the satellite spin axis. The spectrometer had an angular resolution of ±1.5° [*Nightingale et al.*, 1992]. In normal operations the instrument was configured in four different modes, two for electrons and two for protons. It remained in each mode for 32 s. Electron data were also obtained from the IMS-LO spectrometer in three broad energy bands centered at 1.7, 3.9, and 8.9 keV at 75° to the satellite spin axis and with an angular resolution of ±2.5° [*Collin et al.*, 1992]. Further details on these electron spectrometers are available in the referenced papers.

The ion mass spectrometer-higher energy (IMS-HI) instrument [*Voss et al.*, 1992] measured the energy spectra and pitch angle distributions of ions and neutral particles from a few tens of keV to a few hundred keV. The IMS-HI instrument was based on ion momentum separation in a magnetic field followed by a measurement of total energy deposition in a solid-state detector. After exiting the collimators, ions entered a 7000-G magnetic field where they were deflected into various sensors depending on their momentum. Seven cooled (−50°C) solid-state sensors were used in an array at various deflection angles. The instrument featured simultaneous momentum and energy analysis at relatively large geometric factors (between 10^{-3} and 10^{-2} cm^2 sr). The look direction from the spin axis was 75° with a pitch angle resolution of ±2°. The energy range for the proton measurements used here was 18–360 keV.

In the inner radiation belt both SEP and IMS-HI may be sensitive to penetrating protons. Therefore, at $L \leq 2$ the particle fluxes measured by these detectors may have a poorly defined background. Since none of the events discussed in this paper are in the inner zone, this background is not important here.

The electric and magnetic field wave data used in this study were provided by the University of Iowa/Air Force Geophysics Laboratory (AFGL) Plasma Wave Experiment and the University of California at Berkeley/AFGL Electric Field/

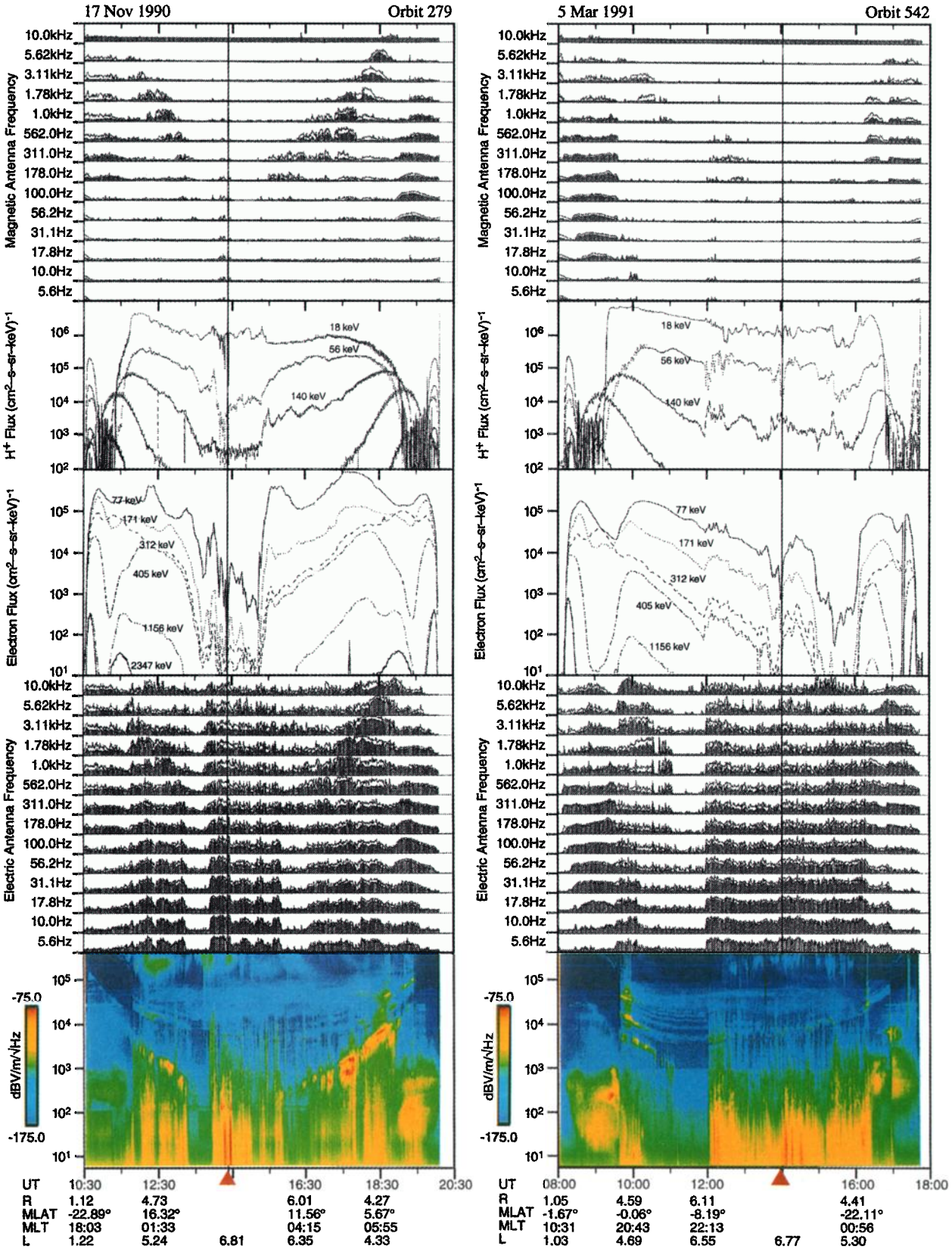

Plate 2. Charged particle and wave data for orbits 279 and 542. The bottom sections contain a sweep frequency receiver spectrogram and the output of the multichannel spectrum analyzer for the electric field wave data. Two other sections contain plots of the fluxes of protons and electrons at various energies averaged over the full range of pitch angles. In a top section the magnetic component of the wave data is plotted. Vertical lines are drawn to show the alignment at the times of special interest.

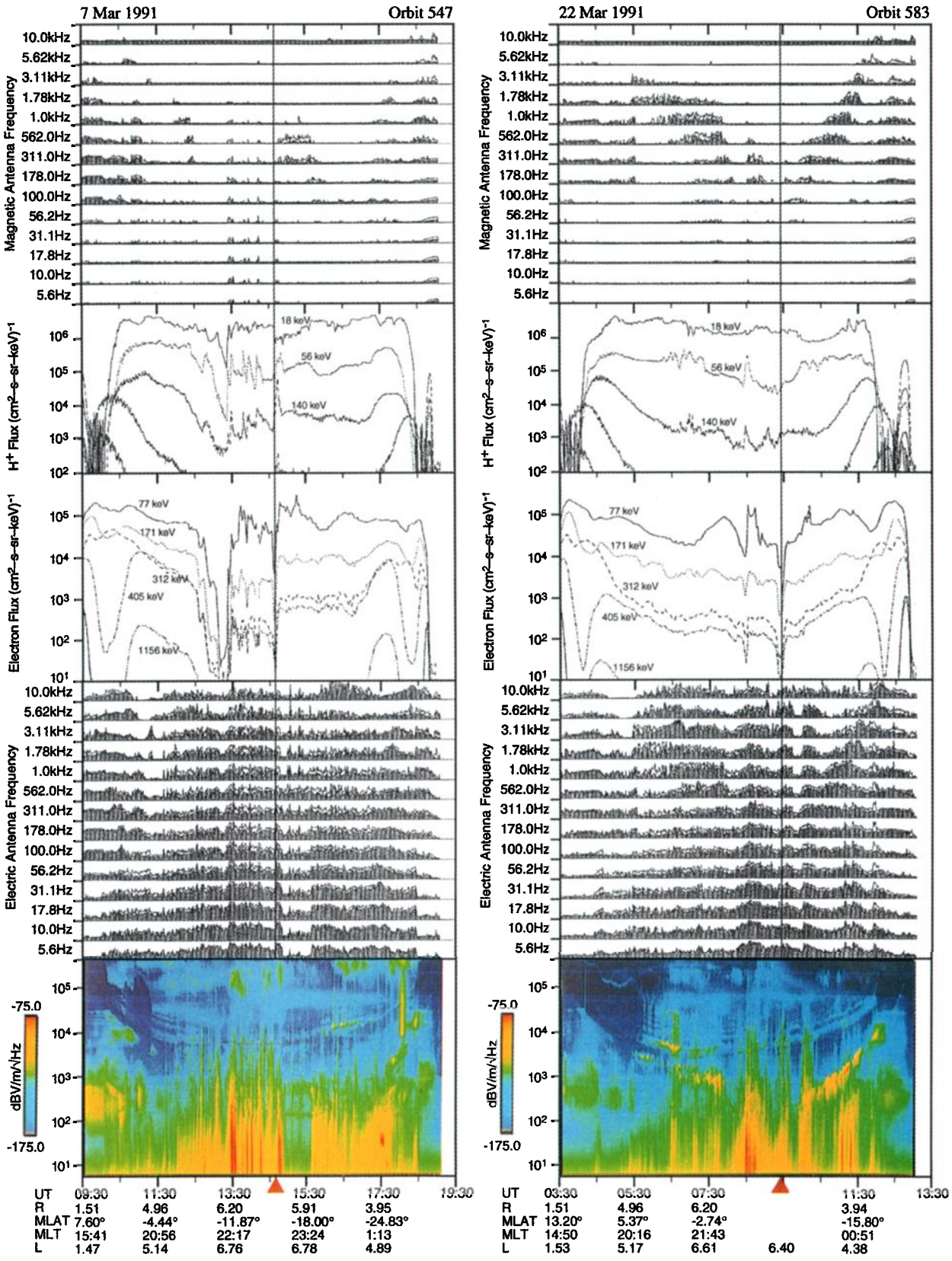

Plate 3. Charged particle and wave data for orbits 547 and 583. The bottom sections contain a sweep frequency receiver spectrogram and the output of the multichannel spectrum analyzer for the electric field wave data. Two other sections contain plots of the fluxes of protons and electrons at various energies averaged over the full range of pitch angles. In a top section the magnetic component of the wave data is plotted. Vertical lines are drawn to show the alignment at the times of special interest.

Langmuir Probe Experiment. The Iowa/AFGL instrument included a sweep frequency receiver (SFR) and multichannel spectrum analyzer (MCA) which together provided electric field wave measurements from 5 Hz to 400 kHz and magnetic field measurements from 5 Hz to 10 kHz [*Anderson et al.*, 1992]. The Berkeley/AFGL experiment [*Wygant et al.*, 1992] measured electric and magnetic waveforms over frequencies ranging from quasi-static to 40 kHz. The instrument also provided continuous monitoring at several samples per second of the wave amplitudes measured through three broadband filters with maximum responses at frequencies of 32, 256, and 2048 Hz.

Electric field wave data in the frequency range 5 Hz to 400 kHz were available during most orbits. Because of an instrument failure the magnetic component of the waves was not measured after orbit 602. Thus, while both electric and magnetic wave amplitudes were compared with particle dropouts up to orbit 602, only electric field intensities could be compared with dropout cases after that orbit.

Examples of Wave and Particle Variations

Since the flux falloffs and recoveries associated with the dropouts have a variety of shapes and amplitudes, a single criterion was used in the selection of narrow dropouts from the electron survey plots. The investigation presented in this paper has been limited to dropouts having an intensity decrease of at least a factor of 10 and an observed duration time for electrons of less than 30 min. Associations of the waves with broader particle dropouts are also observed to occur, but that aspect of the phenomenon has not been studied in this investigation. The selection of dropout cases was made from electron data only and was completed before any comparisons were made with the proton and wave data.

Data From Orbit 186, October 10, 1990

An example of correlated particle and wave data is shown in Plate 1 where selected energetic electron and proton fluxes for the full 10-hour time interval of orbit 186 are plotted in the middle sections of Plate 1. The particle fluxes shown are averaged over the full range of pitch angles. The bottom section of Plate 1 is a spectrogram (frequency versus time with a color code for intensity) from the Iowa electric field wave instrument during the satellite pass. The electron cyclotron frequency Fce determined from the magnitude of the ambient magnetic field measured by the CRRES Magnetometer Experiment [*Singer et al.*, 1992] is indicated by the thin red line drawn across the plot. The magnetic and electric field wave data in 14 frequency channels are plotted separately in different sections. On this orbit, CRRES exited the plasmasphere through a very steep plasmapause at 0638 UT when $L = 3.0$, $R = 2.70\ R_E$, magnetic local time (MLT) = 1.0 hours, and the magnetic latitude was 15°. It reentered the plasmasphere through a very steep plasmapause at 1458 UT when $L = 2.8$, $R = 2.40\ R_E$, MLT = 10.0 hours, and the magnetic latitude was 20°. Geomagnetic activity was high throughout orbit 186. The NOAA World Data Center A for Solar Terrestrial Physics geomagnetic and solar data [*Coffey*, 1991] in fact identified October 10 as the most geomagnetically disturbed day of the month with the 24-hour sum of *Kp* being 37+. October 8 had been the second quietest day of the month with the 24-hour sum of *Kp* being 8+ and the 24-hour sum of *Kp* was 19 for October 9.

The high time resolution electric and magnetic field spectrum analyzer plots from 5 Hz to 10 kHz and electric field spectrograms that extend to 400 kHz show the following features. The primary naturally occurring electromagnetic phenomenon inside the plasmasphere is a broadband isotropic plasmaspheric hiss band between 100 Hz and a few kilohertz. The whistler mode hiss emissions are most likely amplified by anisotropies in the radiation belt electrons. A band of chorus between 100 Hz and 10 kHz extends across the plasmapause crossing at 0638 UT. This band intensified at the leading edge of the dropout at 0735 UT. It did not continue after the dropout as is best seen in the topmost section of Plate 1. Beginning at about 0705 UT the electron cyclotron harmonic (ECH) waves in the band just above Fce and electrostatic ELF waves from 5 Hz to a few hundred hertz intensified. Sporadic electrostatic bursts in the 1–10 kHz range also began around 0705 UT. Around 0725 UT, immediately before the particle dropout, the electrostatic ELF band disappeared or diminished in intensity by more than 2 orders of magnitude. This band reappeared 10 min later at the leading edge of the narrow particle dropout. In fact, at 0735 UT there was a broadband peak in both the electric field noise and the magnetic field noise from 5 Hz up to 10 kHz. These narrow bursts of noise are probably related to the currents which are responsible for a noticeable deflection in the magnetic field at 0735 UT (H. J. Singer, personal communication, 1995). The electrostatic ELF band and higher-frequency electrostatic noise continued after the dropout. Weak impulsive bursts of electromagnetic noise across much of the spectrum analyzer band (5 Hz to 10 kHz) occurred occasionally after the dropout.

The intensification of the ECH waves and the electrostatic ELF waves as well as the occurrence of the sporadic electrostatic waves and electromagnetic chorus in the period from around 0705 UT to nearly 0735 UT is most likely related to the injection of electrons as indicated at that time in the 77 keV electron data shown in Plate 1.

Many wave aspects near the inbound plasmapause crossing at 1458 UT were similar to those previously noted at the outbound crossing. An electromagnetic broadband hiss band extending from around 30 Hz to above 5 kHz was in its mid-frequency range 1–2 orders of magnitude more intense inside the plasmasphere than it was immediately outside the plasmapause. A strong chorus band began near 1300 UT and rose in frequency from 200 Hz at 1300 UT to 20 kHz at the plasmapause where it ended. This band varied in frequency roughly as r^{-6}. It was especially intense from 1355 to 1420 UT. The second short-term dropout in the electron data was centered on 1250 UT. For nearly 1 hour prior to the dropout only a narrow electromagnetic band from 56 to 311 Hz was evident in the magnetic field data. The strong chorus band with the r^{-6} dependence began immediately following the narrowband dropout. The electron data show that a weak electron injection occurred around 1100 UT when the narrowband electromagnetic emissions began. Immediately following the narrowband dropout another electron injection occurred that increased the fluxes several orders of magnitude over the previous injection. These electron fluxes are probably responsible for the chorus band.

Other Examples of Waves Associated With Dropouts

A detailed examination of the wave and particle data has just been made for one complete orbit in which several pronounced variations were observed. In order to achieve a larger statistical sample for the wave and particle comparisons, data are now

presented from 12 orbits in which electron flux dropouts with short observation times occurred. These data are provided in Plates 2–5. The electric field wave data are presented in the bottom sections in the form of spectrograms from the sweep frequency receiver and in other panels as plots of the output of the multichannel spectrum analyzer. For the orbits before 602 the magnetic field wave data are presented in a top section. Fluxes of particles at selected energies averaged over the full range of pitch angles are plotted. Arrows are shown below the sweep frequency receiver data to indicate the times of the selected narrow electron flux dropouts. At these times, vertical lines are drawn through much of the data. It should be noted that on occasion one or more of the instruments are not acquiring data due to spacecraft moding. The electric field wave and electron flux data are plotted on an e xpanded timescale in Plate 6 for four orbits.

The criteria used for selection of dropouts were that they be very pronounced and of short duration (<30 min). This restriction led to a very limited number of cases such that it was not practical to analyze different categories of dropouts separately in various *Kp* and MLT intervals. Since the maximum *Kp* over the previous 24 hours was 4 or greater in all of the cases, it is reasonable to identify all of the events as occurring during geomagnetically disturbed times. The MLT range of the dropouts was also limited, being concentrated in the midnight sector. Consequently, information on the MLT distribution of the short-dropout phenomena is not available.

The examples of Plates 2–6 illustrate the general correlation of waves with particle dropouts as well as the lack of consistent one-to-one correspondence of individual wave bursts with particle fluctuations. The proton flux reductions often took place simultaneously with the electron dropouts, for example, in orbits 279, 542, and 766 but not in 583 and 902. Wave enhancements occurred in the regions of isolated particle dropouts as well as in other regions where the particle fluxes varied rapidly. For example, orbit 615 had multiple occurrences of wave bursts over a 3-hour period during which time the proton and electron fluxes changed erratically.

In almost every case, strong low-frequency electric field turbulence was observed at or very near the time of the narrow dropouts as is most easily seen in the spectrograms. All of the orbits with dropouts prior to orbit 602 showed enhanced low-frequency electromagnetic bursts at or near the time of the dropouts except for orbit 583, as shown in Plate 3. On orbit 583, strong low-frequency electrostatic and electromagnetic emissions were observed associated with what appears to be the start of a narrow flux dropout in the electron data about 0830 UT. The electromagnetic bursts evident around 0930 UT began higher in frequency than those observed for the majority of the narrow dropouts. Inspection of the high time resolution data for all of the orbits showed that the most intense wave activity usually occurred at steep flux density gradients at the leading and trailing edges of the narrow dropouts.

Frequently bands of chorus were observed either just prior to or just after the narrow dropouts. This phenomenon is illustrated in Plate 3 for orbits 547 and 583 (and for orbit 547 in Plate 6) where chorus begins immediately after the narrow dropouts. The appearance or disappearance of chorus after a narrow dropout may indicate that the spacecraft has crossed a boundary into a different region.

On orbit 186 shown in Plate 1 electromagnetic chorus preceded the first narrow dropout (see MAG Antenna panel) and did not continue immediately after the dropout. For the second dropout, chorus was sharply enhanced after the narrow dropout. On orbits 279 and 542 shown in Plate 2 (also in Plate 6 for orbit 542) chorus was not associated with the dropouts. On orbit 279 the chorus ended near 1330 UT as the fluxes of the highest energy electrons fell dramatically. It reappeared about 1530 UT when the fluxes of highest-energy electrons increased dramatically. On orbit 542 the chorus ended around 1100 UT when the electron fluxes gradually dropped as the spacecraft moved to the outer portion of the outer radiation belt. The chorus reappeared suddenly about 1200 UT at the time electron flux levels increased enough to sustain chorus generation. Then chorus diminished again around 1300 UT as the flux levels continued to fall. During these injections the outer magnetosphere apparently has sufficient plasma to support intense electromagnetic waves.

For orbit 615 shown in Plate 4 it is clear that the electric field emissions associated with the boundaries of the narrow dropouts just after 1100 UT are very similar to various emissions throughout the interval 1100–1300 UT including those associated with the narrow spike in the electron flux just after 1000 UT. In Plate 4, orbits 615 and 666 show examples of narrow dropouts occurring in the middle of a region of plasma generating strong electric field noise. Orbits 686 and 737 (in both Plates 4 and 6) also show examples of narrow dropouts at the boundary leading into a region generating intense electric field noise.

The data for orbit 759 in Plate 5 illustrate the similarity of the electric field waves in a narrow dropout region to those associated with a sudden injection of plasma. For orbit 766 we see how intense the electric field waves are for strong and continuous injections of both electrons and protons. For orbit 766 we see that a period of very little wave activity also preceded the plasma injection occurring just before 0730 UT.

Short-Term Fluctuations

For investigation of shorter timescales (Δt < 30 min) the electric field wave data at three different frequencies are plotted in the top sections of Figures 1 and 2 for a 1-hour interval. For the investigation of short-term fluctuations the proton measurements from IMS-HI were used in preference to the electrons measured with the SEP instrument whose time resolution was 2 min. In the lower two sections of Figure 1 are plotted the fluxes of protons at 18 and 56 keV averaged over the full range of pitch angles.

While some individual wave bursts occur simultaneously (within ≈ 15 s) with the proton changes (for example, the bursts at 1400:30 in Figure 1 and at 0515:15 in Figure 2), numerous wave bursts of about 30-s duration have no association with proton changes.

The data from the three filters presented in Figures 1 and 2 indicate that the rms amplitude of the electric field is often stronger in the lower-frequency filters than the higher-frequency filters. The electric field fluctuations reach amplitudes of 5–10 mV/m during periods of peak power. Comparisons of the sinusoidal modulation of the filter outputs (at twice the spacecraft spin period) to the orientation of the electric field booms relative to the ambient magnetic field direction indicate that the fluctuation amplitude is greatest when the booms are perpendicular to the magnetic field direction. These comparisons imply that the waves are predominantly polarized perpendicular to the magnetic field during these events. It should be noted that the filters average the fluctuation amplitude of the electric field over one second, and the peak am-

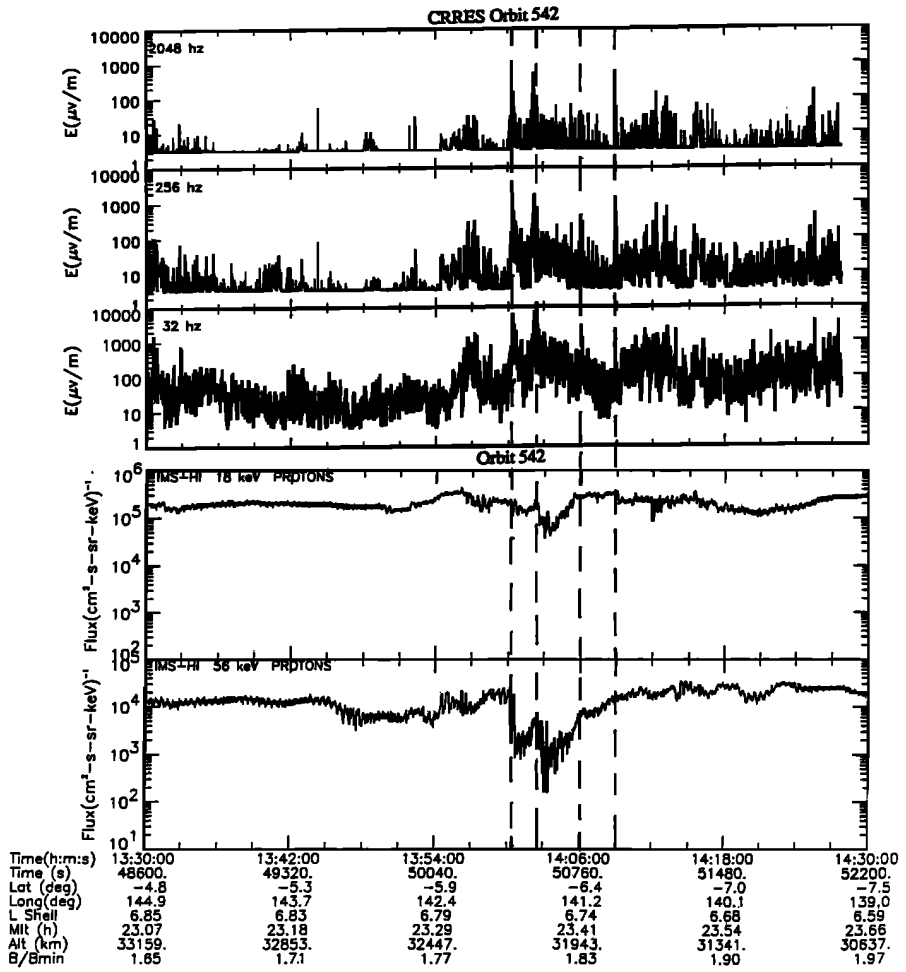

Figure 1. Proton and wave data for a portion of orbit 542. In the top sections the electric field wave intensities at three different frequencies are plotted. In the bottom sections are plotted the fluxes of protons at 18 and 56 keV averaged over the full range of pitch angles. Vertical lines are drawn to show the alignment at times of special interest.

plitudes measured with higher time resolution can be significantly higher.

Each of the narrow energetic electron dropouts selected in the survey of the CRRES data is listed in Table 1. All of these narrow dropouts had observation durations of less than 30 min. Table 1 lists several quantities associated with the start of recovery from the dropout: universal time in hours, MLT, L, Kp, and Dst. The presence or absence of a dropout in the ions is indicated. Two columns indicate whether there was a change in the VLF electrostatic or electromagnetic wave intensity. High-energy ion dropouts occurred simultaneously with electron dropouts in more than half of the cases, whereas low-energy ion dropouts were present during only about a quarter of the electron dropouts.

Discussion

The data presented here have shown the general correlations between wave intensities and particle fluxes. The most pronounced correlations occurred at the times of new particle injections or plasmapause crossings. Strong wave intensities frequently occurred in association with broad dropouts at the time of substorms. However, the principal objective of this paper has been to study the interesting phenomena of narrow particle dropouts which have been found frequently to be associated with wave enhancements.

The energetic particle dropouts are caused by the satellite suddenly entering a substantially different plasma environment having much less ($<10^{-1}$) particle flux than experienced immediately before or after the dropout. These flux changes often but not always occurred for all energetic particle types observed. However, the time profiles of the particle flux are sometimes quite different for electrons and protons. One would expect slightly different boundaries for the various species and energies since the different populations have different gyroradii and drift velocities. Also, the ions and electrons drift in opposite directions. In some cases the thermal plasma also showed a strong density reduction, as would be expected if the satellite passed into field lines leading to the tail. The magnetic field frequently increased during the particle dropouts in agreement with the expected diamagnetic behavior of the plasma.

A coarse timescale ($\Delta t \geq 30$ min) comparison of wave and particle intensities during the time interval surrounding the dropout events reveals that a general increase in wave intensity

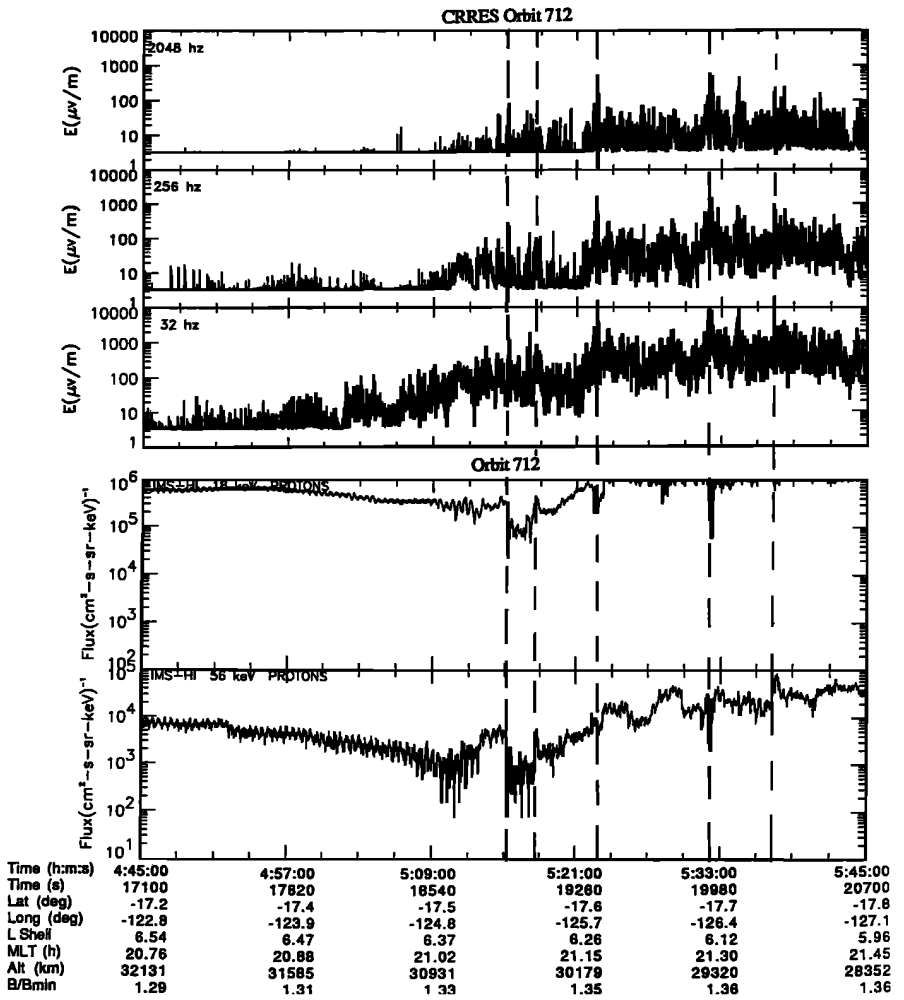

Figure 2. Proton and wave data for a portion of orbit 712. In the top sections the electric field wave intensities at three different frequencies are plotted. In the bottom sections are plotted the fluxes of protons at 18 and 56 keV averaged over the full range of pitch angles. Vertical lines are drawn to show the alignment at times of special interest.

for 5 Hz < frequency < 1 kHz occurs at or near the time of each dropout. The occurrence of wave bursts is so infrequent that their association with particle flux changes cannot be by chance. In the course of this investigation of narrow dropouts some broad dropouts were also examined, and it was discovered that wave enhancements often occurred near the edges of the broad dropout at times of sharp decreases or increases in energetic particle flux. The association of waves and particle dropouts is not perfect, however. While wave enhancements almost always occur near the dropouts, bursts of wave activity are sometimes seen at times when there are no observable changes in particle fluxes. This finding may be attributed to the narrow localization of the particle fluxes in comparison with the more widespread nature of the waves.

A detailed comparison of waves and particles on very short timescales ($\Delta t < 30$ s) shows a much weaker correlation. In some cases a sudden change in particle flux (at the edge of the dropout) coincided with a pronounced change in the wave environment (see, for example, orbits 279 and 542), although in many cases the initial times were several seconds apart. Some flux features, peaks or valleys, as short as 15-s duration appeared to coincide with enhanced or reduced wave amplitude. In these cases, an increased particle flux sometimes accompanied an increase in wave amplitude and sometimes a reduced wave amplitude. Most of the time, however, the detailed structure of the particle fluxes (feature less than 30 s long) did not correspond consistently with wave data.

We interpret the coarse timescale observations in association with narrow particle dropouts as indicative that waves are produced at or near the particle boundaries which define the sudden flux changes. These waves propagate some distance from the generation site, and hence only a general correlation with particle boundaries is observed. The probability of detecting the waves depends both on the generation strength as well as the propagation path and will therefore depend on the detailed plasma properties and geometry in particular cases. For fine scale observations the lack of a consistent correlation between the waves and the particle fluxes may result from the difference in spatial extent of the two quantities.

An alternate interpretation might be constructed in which the waves scattered the particles and thereby produced the sudden reductions in trapped flux. This possibility appears very unlikely in that a resonance interaction would not be expected to affect all particle types over a broad range of energies si-

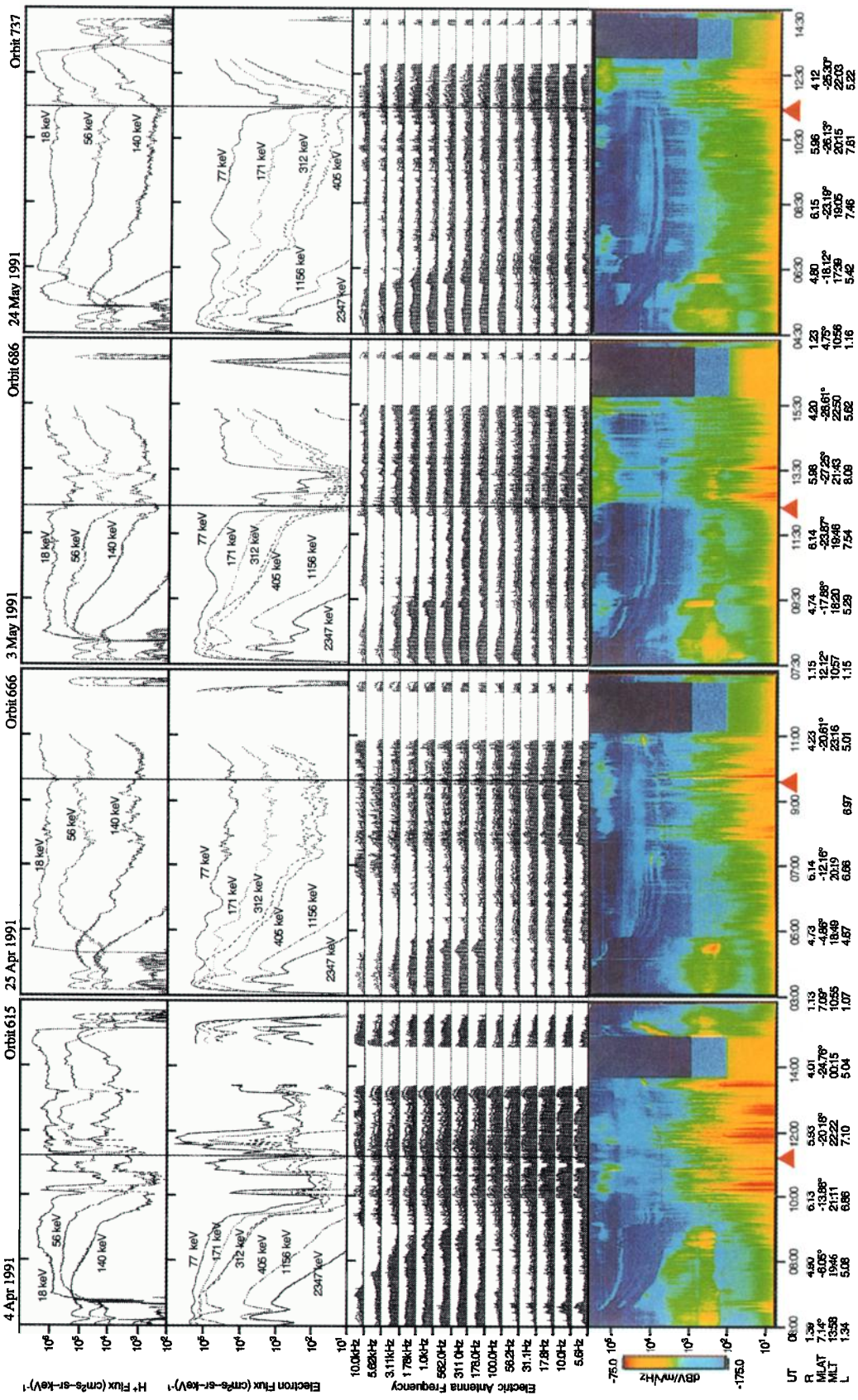

Plate 4. Charged particle and wave data for orbits 615, 666, 686, and 737. The bottom sections contain a sweep frequency receiver spectrogram and the output of the multichannel spectrum analyzer for the electric field wave data. Two other sections contain plots of the fluxes of protons and electrons at various energies averaged over the full range of pitch angles. Vertical lines are drawn to show the alignment at the times of special interest.

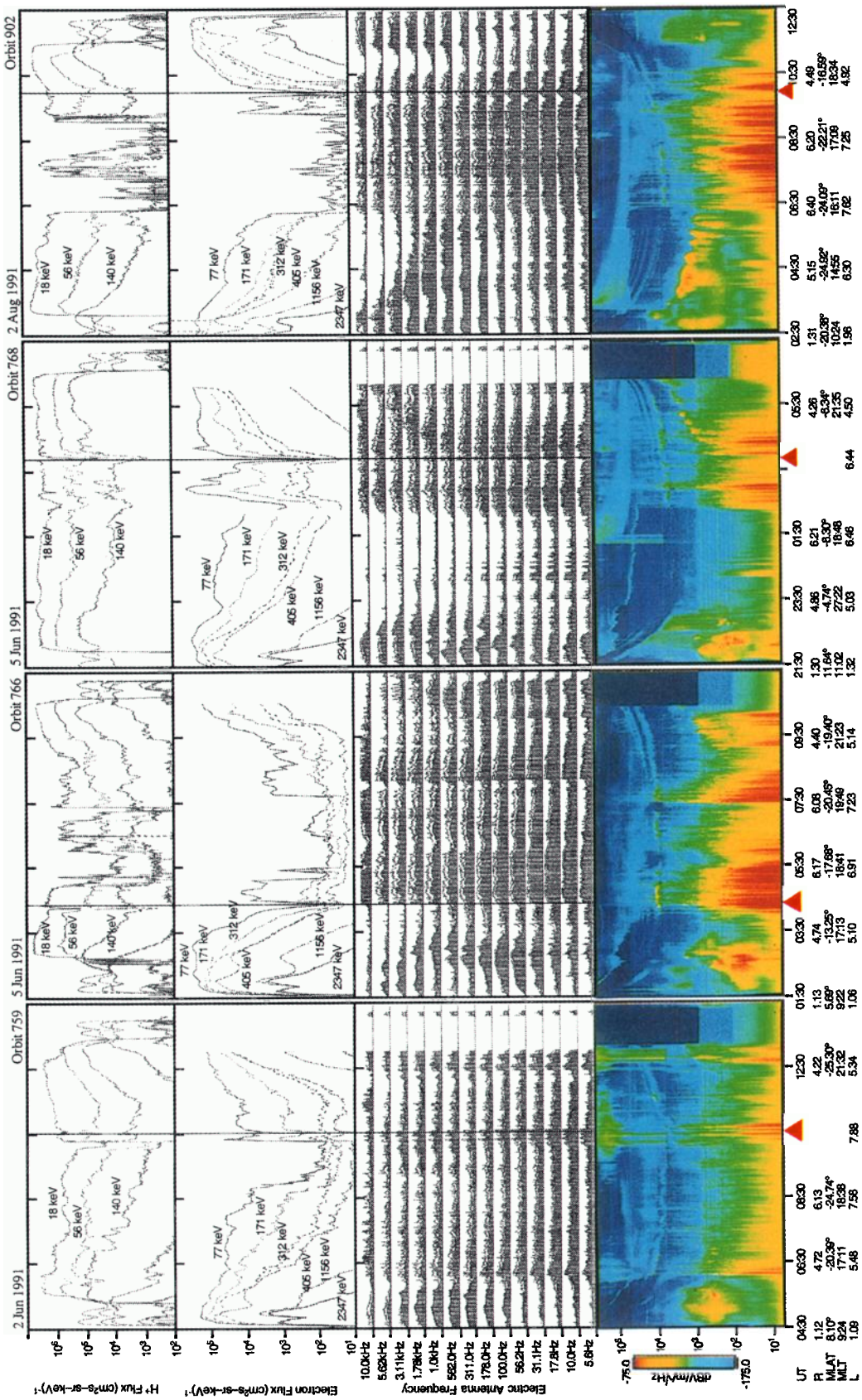

Plate 5. Charged particle and wave data for orbits 759, 766, 768, and 902. The bottom sections contain a sweep frequency receiver spectrogram and the output of the multichannel spectrum analyzer for the electric field wave data. Two other sections contain plots of the fluxes of protons and electrons at various energies averaged over the full range of pitch angles. Vertical lines are drawn to show the alignment at the times of special interest.

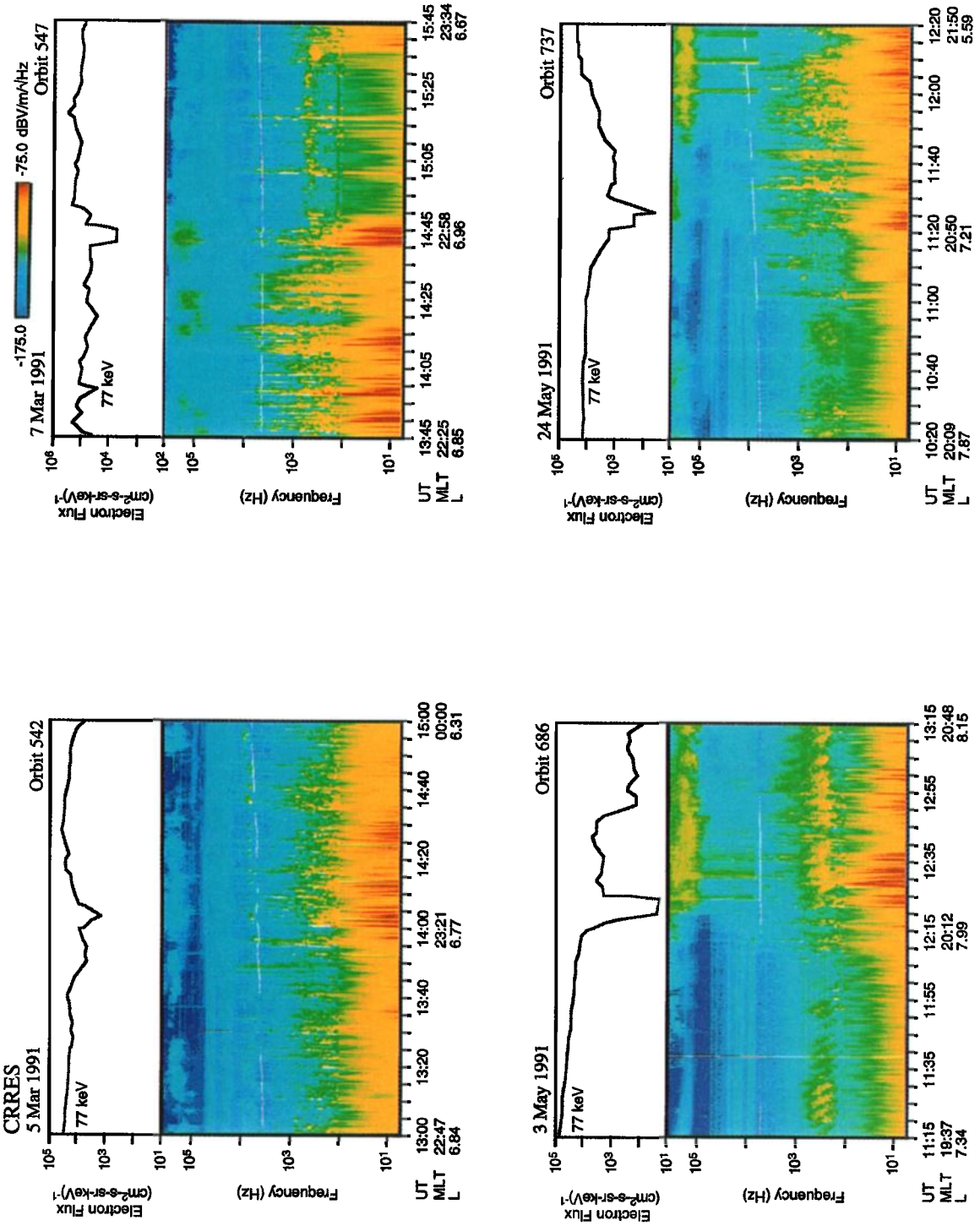

Plate 6. Sweep frequency receiver spectrograms and electron flux at 77 keV on orbits 542, 547, 686, and 737 for 2-hour periods roughly centered on the times of the narrow particle dropouts.

Table 1. Characteristics of Narrow Electron Dropouts <30 min

Start of Recovery From Electron Dropout							Maximum *Kp* in Previous 24 Hours	VLF Electric Field Wave Change	VLF Magnetic Field Wave Change	Ion Dropout	
Orbit	Date	UT	MLT	*L*	*Dst*	*Kp*				>18 keV	<10 keV
186	Oct. 10, 1990	0737	0254	5.41	−114	6	6	yes	yes	yes	yes
186	Oct. 10, 1990	1249	0630	7.20	−88	5	6	no	no	no	no
279	Nov. 17, 1990	1424	0254	6.76	−36	4	4	yes	yes	yes	...
542	March 5, 1991	1402	2324	6.76	−30	4	5−	yes	yes	yes	no
547	March 7, 1991	1443	2300	6.96	−20	4−	5	yes	yes	no	no
552	March 9, 1991	1734	2354	6.24	−30	3+	4+	yes	yes	yes	no
583	March 22, 1991	0925	2254	6.43	−38	4	7−	weak	yes	no	...
615	April 4, 1991	1113	2154	7.22	−3	6+	6+	yes	na	yes	no
666	April 25, 1991	0930	2154	6.75	−21	3	5−	yes	na	yes	yes
686	May 3, 1991	1223	2018	8.05	−22	3	6	yes	na	yes	...
712	May 14, 1991	0517	2106	6.29	−28	3+	5	weak	na	yes	no
719	May 17, 1991	0046	2012	6.61	13	6	6	no	na	no	no
737	May 24, 1991	1125	2054	7.07	−19	2+	5−	yes	na	no	no
759	June 2, 1991	1029	1948	7.89	−43	4	7+	yes	na	no	...
766	June 5, 1991	0413	1748	5.95	−76	7+	7+	yes	na	yes	no
768	June 6, 1991	0354	1830	6.68	−147	6−	9−	yes	na	yes	yes
902	Aug. 2, 1991	0953	1800	5.98	−91	5+	6+	yes	na	no	no

Three center dots denote insufficient ion flux to establish the presence of a dropout; na, data not acquired.

multaneously. Furthermore, even in the strong diffusion limit with the loss cone filled, the overall particle loss rate is limited by the number of particles in the loss cone as they reach the atmosphere. Because of the small size of the loss cone at the satellite position for these data, over 1.5 min would be required to deplete the electron population, and several hours would be needed for the protons.

Acknowledgments. The SEP, IMS-LO, and IMS-HI instruments are part of the ONR307 experiment on CRRES, and much of the data analysis presented here was sponsored by the Office of Naval Research (contracts N00014-83-C-0476 and N00014-94-C-0042). The Lockheed Independent Research Program provided partial support for the analysis. Special thanks are extended to J. P. McGlennon and J. Beeler for their dedicated data analysis contributions. Interactions with H. J. Singer were very helpful. Appreciation is given for the contribution of R. R. Vondrak. The research effort at the University of Iowa has been supported by NASA under subcontract 9-X29-D9711-1 with Los Alamos National Laboratory. Special thanks go to R. W. Lane for his programming efforts and to M. D. Brown for producing the wave data plots. The University of California, Berkeley work was performed under Air Force contract F19628-92-K-0009.

The Editor thanks A. Korth and M. F. Thomsen for their assistance in evaluating this paper.

References

Anderson, R. R., D. A. Gurnett, and D. L. Odem, CRRES plasma wave experiment, *J. Spacecr. Rockets*, *29*, 570–573, 1992.

Baker, D. N., and R. L. McPherron, Extreme energetic particle decreases near geostationary orbit: A manifestation of current diversion within the inner plasma sheet, *J. Geophys. Res.*, *95*, 6591–6599, 1990.

Baker, D. N., T. I. Pulkkinen, R. L. McPherron, J. D. Craven, L. A. Frank, R. D. Elphinstone, J. S. Murphree, J. F. Fennell, R. E. Lopez, and T. Nagai, CDAW 9 analysis of magnetospheric events on May 3, 1986: Event C, *J. Geophys. Res.*, *98*, 3815–3834, 1993.

Coffey, H. E., Geomagnetic and solar data, *J. Geophys. Res.*, *96*, 1885, 1991.

Collin, H. L., J. M. Quinn, G. R. Smith, E. Hertzberg, S. Roselle, and S. J. Battel, The low-energy ion spectrometer on CRRES, *J. Spacecr. Rockets*, *29*, 617–620, 1992.

Erickson, K. N., R. L. Swanson, R. J. Walker, and J. R. Winckler, A study of magnetosphere dynamics during auroral electrojet events by observations of energetic electron intensity changes at synchronous orbit, *J. Geophys. Res.*, *84*, 931–942, 1979.

Fennell, J., J. Roeder, H. Spence, H. Singer, A. Korth, M. Grande, and A. Vampola, CRRES observations of particle flux dropout events, *Adv. Space Res.*, *18*(8), 217–228, 1996.

Kaufmann, R. L., J. T. Horng, and A. Konradi, Trapping boundary and field-line motion during geomagnetic storms, *J. Geophys. Res.*, *77*, 2780–2798, 1972.

Kopanyi, V., and A. Korth, Energetic particle dropouts observed in the morning sector by the geostationary satellites GEOS-2, *Geophys. Res. Lett.*, *22*, 73–76, 1995.

Korth, A., R. Friedel, D. N. Baker, H. Luhr, S. L. Ullaland, J. F. Fennell, and G. D. Reeves, Dynamics of the plasma sheet in the dawn sector of the magnetosphere: Observations from CRRES, in *Proceedings of International Conference on Substorms 2*, edited by J. R. Kan, J. D. Craven, and S. I. Akasofu, p. 315, Geophys. Inst., Fairbanks, Alaska, 1995.

Moldwin, M. B., M. F. Thomsen, S. J. Bame, D. J. McComas, and J. Birn, Flux dropouts of plasma and energetic particles at geosynchronous orbit during large geomagnetic storms: Entry into lobes, *J. Geophys. Res.*, *100*, 8031–8043, 1995.

Nagai, T., Local time dependence of electron flux changes during substorms derived from multi-satellite observations at synchronous orbit, *J. Geophys. Res.*, *87*, 3456–3468, 1982.

Nakamura, R., D. N. Baker, T. Yamamoto, R. D. Belian, E. A. Bering III, J. R. Benbrook, and J. R. Theall, Particle and field signatures during pseudobreakup and major expansion onset, *J. Geophys. Res.*, *99*, 207–221, 1994.

Nightingale, R. W., R. R. Vondrak, E. E. Gaines, W. L. Imhof, R. M. Robinson, S. J. Battel, D. A. Simpson, and J. B. Reagan, The ONR-307-3 spectrometer for electrons and protons on the CRRES Satellite, *J. Spacecr. Rockets*, *29*, 614–617, 1992.

Sauvaud, J. A., and J. R. Winckler, Dynamics of plasma, energetic particles, and fields near synchronous orbit in the nighttime sector during magnetospheric substorms, *J. Geophys. Res.*, *85*, 2043–2056, 1980.

Sauvaud, J. A., and T. Beutier, On the origins of flux dropouts near geosynchronous orbit during the growth phase of substorms, 1, Betatron effects, *J. Geophys. Res.*, *101*, 19911–19919, 1996.

Sergeev, V. A., T. Bosinger, R. D. Belian, G. D. Reeves, and T. E. Cayton, Drifting holes in the energetic electron flux at geosynchronous orbit following substorm onset, *J. Geophys. Res.*, *97*, 6541–6548, 1992.

Singer, H. J., W. P. Sullivan, P. Anderson, F. Mozer, P. Harvey, J. Wygant, and W. McNeil, Fluxgate magnetometer instrument on the CRRES, *J. Spacecr. Rockets*, *29*, 599–601, 1992.

Su, S.-Y., T. A. Fritz, and A. Konradi, Repeated sharp flux dropouts observed at 6.6 R_E during a geomagnetic storm, *J. Geophys. Res.*, *81*, 245–252, 1976.

Thomsen, M. F., S. J. Bame, D. J. McComas, M. B. Moldwin, and K. R. Moore, The magnetospheric lobes at geosynchronous orbit, *J. Geophys. Res.*, *99*, 17,283–17,293, 1994.

Voss, H. D., E. Hertzberg, A. G. Ghielmetti, S. J. Battel, K. L. Appert,

B. R. Higgins, D. O. Murray, and R. R. Vondrak, Medium energy ion mass and neutral atom spectrometer, *J. Spacecr. Rockets*, *29*, 566–569, 1992.

Walker, R. J., K. N. Erickson, R. L. Swanson, and J. R. Winckler, Substorm-associated particle boundary motion at synchronous orbit, *J. Geophys. Res.*, *81*, 5541–5550, 1976.

Wygant, J. R., P. R. Harvey, D. Pankow, F. S. Mozer, N. Maynard, H. Singer, M. Smiddy, W. Sullivan, and P. Anderson, The CRRES electric field/Langmuir probe instrument, *J. Spacecr. Rockets*, *29*, 601–604, 1992.

Yeager, D. M., and L. A. Frank, Large temporal variations of energetic electron intensities at midlatitudes in the outer radiation zone, *J. Geophys. Res.*, *74*, 5697–5708, 1969.

R. R. Anderson, Department of Physics and Astronomy, University of Iowa, Iowa City, IA 52242.

H. L. Collin, W. L. Imhof, and J. Mobilia, Lockheed Martin Palo Alto Research Laboratory, Palo Alto, CA 94304.

H. D. Voss, Physics Department, Taylor University, Upland, IN 46989.

M. Walt, STARLAB, Stanford University, Stanford, CA 94305.

J. R. Wygant, School of Physics and Astronomy, University of Minnesota, Minneapolis, MN 55455.

(Received July 31, 1996; revised February 6, 1997;
accepted February 7, 1997.)